

Experimental validation of a corner stall control methodology using parametrised guide fins

Review article

Article history:

Submission date: 9 May 2022

Acceptance date: 20 July 2022

Publication date: 28 September 2022

This is the updated version of a paper originally presented at the Global Power and Propulsion Virtual Technical Conference, GPPS Xi'an21, April 11–13, 2022.



*Correspondence:

XO: xavier.ottavy@ec-lyon.fr

Peer review:

Single blind

Copyright:

© 2022 Safran – William RIERA, Gabriel MONDIN, Pierre DUQUESNE, Xavier OTTAVY © This is an open access article distributed under the Creative Commons Attribution Non Commercial No Derivatives License (CC BY-NC-ND 4.0). Unrestricted use, distribution, and reproduction of the original work are permitted for noncommercial purposes only, provided it is properly cited and its authors credited. No derivative of this work may be distributed.

Keywords:

corner stall control; linear compressor cascade; guide fins; RANS-based design

Citation:

Mondin G. J. V., Riéra W., Duquesne P., and Ottavy X. (2022). Experimental validation of a corner stall control methodology using parametrised guide fins. *Journal of the Global Power and Propulsion Society*. 6: 266–278.
<https://doi.org/10.33737/jgpps/152238>

Gabriel Jacques Victor Mondin^{1,2}, William Riéra², Pierre Duquesne¹, Xavier Ottavy^{1,*}

¹Univ Lyon, LMFA UMR5509, Ecole Centrale de Lyon, Univ Claude Bernard Lyon 1, INSA Lyon, 69134 Ecully, France

²Energy and Propulsion Department, Safran Tech, Rue des Jeunes Bois, Châteaufort, 78114 Magny-Les-Hameaux, France

Abstract

Corner separation is known to limit the operability of aeronautical compressors. Dedicated control devices such as guide fins are envisioned to reduce its negative effects. This paper presents a methodology based on RANS (Reynolds-Averaged Navier-Stokes) computations enabling to select guide fins efficient for that purpose. This methodology is applied to a reference case of linear compressor cascade operating at low Mach number (~ 0.11). A set of 17 parameters is used to define two design spaces of interest, from which guide fins are generated. From then, an automated process generates and merges an unstructured mesh built around each guide fin with a fixed, structured mesh of reference representing a single channel of the cascade. Finally, RANS results on the resulting hybrid mesh are obtained using the Computational Fluid Dynamics solver elsA. This set up has proven successful in evaluating automatically hundreds of guide fins of various shapes. Several geometries illustrate the diversity of the design space. A selection of guide fins is then evaluated experimentally. Evolutions of the losses downstream of the cascade are compared to their respective RANS predictions, and to the reference case without guide fin. These experimental results validate the implemented methodology and show encouraging results in terms of loss redistribution brought by the control device.

Introduction

Corner separation is a three-dimensional separation occurring at the blade-endwall junction in aeronautical compressors. It is proven to originate from complex interactions of secondary flow structures (Horlock et al., 1966; Kang and Hirsch, 1991), and is one of the most limiting flow feature in modern aeronautical compressors in terms of efficiency and operability. More specifically, the azimuthal pressure gradient that exists between two consecutive blades causes the so-called passage flow in the near-endwall region. This flow drives low momentum fluid towards the suction side of one blade, which accumulates and leads to a high-loss region that can be prone to stall. This high-loss region can be characterised by the topology of the skin friction lines patterns (Délery, 2001). It is greatly influenced by the operating conditions, and notably by the inflow incidence (Taylor and Miller, 2017; Dawkins et al., 2021).

Corner separation is very sensitive to the channel geometry and can be influenced in different ways. The 3D stator design itself is of great importance (Harvey and Offord, 2008; Taylor and Miller, 2017) as well as the type of junctions with which it is embedded to the endwall. The

presence and type of fillets and hub clearance can indeed significantly impact the corner separation (Goodhand and Miller, 2012; Sun et al., 2021). Non-axisymmetric endwall deformation can also be used to smoothly deflect the flow (Reutter et al., 2017) or act as an aerodynamic separator (Hergt et al., 2009). On top of these geometrical modifications, technological devices such as vortex generators or fences can be added (Hergt et al., 2011, 2013). This paper intends to provide a methodology that aims at studying a new type of control device, called “guide fin”, corresponding to one or several profiled fences of potentially non-conventional shape. The idea behind the guide fin is to provide a tuneable control device in between the vortex generator and the non-axisymmetric endwall, which can either lower the losses at near-design conditions or on a broad range of incidences.

In the present work, the guide fins are evaluated in a subsonic linear compressor cascade at the LMFA, Lyon. A key advantage of such a configuration is to allow detailed measurements that precisely characterise the corner separation (Ma et al., 2013; Zambonini et al., 2017; Dawkins et al., 2021). These works, as well as (Feng et al., 2015), showed that low fidelity computations such as RANS have difficulties in predicting the corner separation size. According to (Lei et al., 2008), RANS can predict two topologies of corner separations, referred to as *closed* and *open*. (Taylor and Miller, 2017) showed that at the critical incidence, a pair of saddle and focus critical points appears at the blade – endwall junction, and rapidly moves away from the blade suction side. As a consequence, the corner separation switches from the *closed* to the *open* topology, yielding a sudden increase in losses and blockage. However, (Dawkins et al., 2021) measured a smooth evolution of the experimental losses with the incidence, proving that the notion of critical incidence is purely numerical. Such a defect in RANS predictions can be explained by the anisotropy of the Reynolds stress tensor in the corner region (Gessner, 1973), not accounted for when using the Boussinesq hypothesis.

However, time-averaged friction lines from (Dawkins et al., 2021) show that this saddle/focus pair exists, but appears at an incidence between 0.8° and 2.3° in the baseline considered in this paper. Before the appearance of this pair, time-averaged friction lines are very similar to what RANS predicts, bringing confidence in RANS predictions at near-design incidences. Moreover, (Dawkins et al., 2021) showed that the flow anisotropy in the corner region increases with the incidence, together with total pressure losses. In this work, the studied control device aims at reducing the separation magnitude, which might help reducing the flow anisotropy. In other words, best guide fins in terms of loss reduction could be the best predicted ones. On the other hand, non-efficient guide fins could lead to similar loss over predictions than with the *open* topology, and would be discarded.

RANS could then be fitted to evaluate control devices that reduce the corner separation size. A RANS-based numerical methodology is thus proposed in this paper to explore the effect of numerous guide fins on a baseline configuration. It relies on an automated numerical chain in which parametrised guide fins are generated, included in a mesh of reference and evaluated using RANS computations. Two sub-domains of the design space are explored and several guide fins improving the flow at two incidences are found. Experimental measurements involving two of these guide fins are finally presented and validate the numerical methodology by showing a significant loss reduction.

Experimental set up

Baseline configuration

The experiments were performed in a subsonic cascade wind tunnel at the LMFA, Lyon, whose characteristics are precisely detailed by (Dawkins et al., 2021). This cascade is set in order to precisely control the inlet flow, which consists in the inlet endwall boundary layer, the inlet angle and the inlet turbulence. The cascade parameters are presented in Table 1. Bleeding channels are used to remove the boundary layer developing on the endwall 0.5 stator chord (c) upstream of the channels. For each flow condition, the bleeding flow is altered to retrieve the same pressure profile around the endwall leading edge. This set up ensures a thin and repeatable inlet boundary layer for all inflow conditions. This enables to observe a classical, repeatable corner separation behaviour downstream of the cascade. 25 pressure tapings are used to best fit the pressure distribution along the profile at midspan against a database of numerical flow predictions obtained at angle increments of 0.1° . This enables to measure the inflow incidence with a precision of $\pm 0.05^\circ$ for the investigated blade. The inlet turbulence is generated by a grid 280 bar widths upstream of the cascade and measured $0.25c$ upstream of the leading edge of the blades.

The performance of the cascade is measured with a five-hole probe (P_t) in a plane at $0.2c$ downstream of the trailing edge, along with inlet pitot tubes ($P_{s,\infty}$, $P_{t,\infty}$) for inflow pressures reference. Their respective positions are

Table 1. Cascade Characteristics.

Cascade parameters	Value
Profile type	Controlled diffusion
Chord	125 mm
Pitch	70.6 mm
Span	290 mm
Design inflow angle	52.8°
Blade Stagger	35.4°
Inlet metal angle	59.0°
Outlet metal angle	22.5°
Chord-based Reynolds number	$3.2 \cdot 10^5 \pm 0.15\%$
Inlet Mach number	0.11
Inlet Turbulence rate	$2.4\% \pm 0.1\%$
Inlet Momentum thickness θ/c	$0.0030 \pm 6\%$

shown in Figure 1. The total pressure losses are computed as

$$\omega = -C_{p,t} = \frac{P_{t,\infty} - P_t}{P_{t,\infty} - P_{s,\infty}} \quad (1)$$

The integrated pressure losses ω_T are defined as the mass-averaged pressure losses on the whole plane of measurement. The profile losses ω_{MID} are defined as the mass-averaged pressure losses at the same axial position, but at midspan only. The endwall pressure losses are defined as the difference between the integrated pressure losses and the profile losses:

$$\omega_{EW} = \omega_T - \omega_{MID} \quad (2)$$

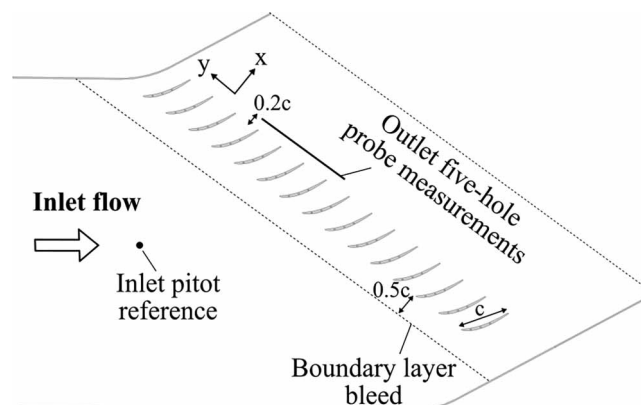


Figure 1. Side view of the rig.

This baseline configuration is intended to be used as an open test case for corner separation studies, and was precisely designed and characterised by (Dawkins et al., 2021) for that purpose. The high aspect ratio of the blade is made on purpose to uncouple the midspan flow from the near-endwall flow and to isolate the corner separations occurring at the two roots of the blade. The midspan profile trailing edge separation starts at the incidence $i = 5.5^\circ$, and develops further upstream as the incidence is increased. Moreover, endwall losses rapidly increase with the incidence, from approximately 0.9% at $i = 0^\circ$ to 4.3% at $i = 5.4^\circ$, and are obtained with an experimental uncertainty of $\pm 0.1\%$. This is shown later in the Results and Discussion section. As such, this precisely controlled cascade exhibits an important corner separation, and can therefore be used for evaluating a control device such as guide fins.

Guide fin manufacturing and insertion

An insertion system was designed to equip six neighbouring channels with guide fins, on both endwalls. It is made of a fixed part fitting the stator profile in which a removable part containing the guide fin can be slid in. Figure 2 illustrates this principle, and Figure 3 its implementation in the cascade. The system is 2 mm thick, yielding a section reduction of about 1.3%. Its upstream part starts at an axial position $0.29c$ upstream of the stator leading edge. It consists of a ramp that smoothly brings the flow up, from the endwall to the top of the platform, with an angle seen by the flow of 3.8° . This system, including the guide fin, is manufactured with a Fuse Deposition Modelling (FDM) method, using ABS plastic. A nozzle of 0.4 mm diameter is used, as well as a precision of 0.09 mm per layer. With this system, a complete set of 12 guide fins is manufactured in about 30 hours, which is much faster than with a conventional process. In order to limit extra losses and the inlet boundary layer thickening, the fixed part is sanded down to a rugosity of $0.5 \mu\text{m}$. The same operating points are reached with and without the insertion system. Nonetheless, adding this system necessarily alter the reference flow. A flat platform was then slid in the insertion system to mimic the initial baseline configuration. This modified baseline is characterised experimentally by the authors, and is the one used in this paper. This way, the gain measured when replacing the flat platform by a platform with a guide fin is independent of the insertion system. Moreover, a variation of the endwall losses below the experimental uncertainty is found at several incidences when comparing the initial and modified baseline. This yields a negligible effect of the system.

This experimental set up thus enables to assess the influence of a guide fin on endwall losses. Next section describes a RANS-based methodology implemented to find manufacturable guide fins that efficiently reduce the endwall losses.

Methodology for guide fin generation and evaluation

In order to evaluate numerically numerous guide fins of various shapes, an automated numerical chain is developed. It is composed of three main steps: guide fins parametrisation, mesh generation and CFD computation.

Guide fin parametrisation

In order to ensure an aerodynamic shape, the guide fin is built using several aerofoils stacked at different span-wise locations, from hub to tip. So as to reduce the total number of parameters, it is chosen to build only one

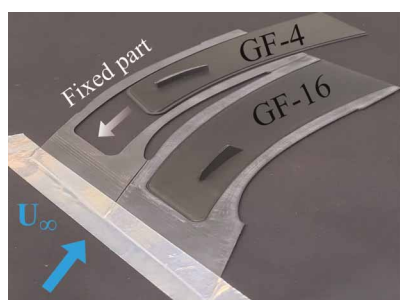


Figure 2. Illustration of the insertion system, with GF-4 and GF-16. U_∞ refers to the upstream velocity.



Figure 3. Rear view of the system in the cascade.

parametrised aerofoil, whose parameters values are a function of its spanwise location. The evolution of each parameter is chosen to be linear, because it requires only two values and still allows the construction of complex geometries. Finally, two fillets can be added to round the junctions between the hub and the sides, and between the tip and the sides. Examples of guide fins generated with the following methodology are shown in Figure 4.

Aerofoil parametrisation

The parametrised aerofoil is built from a parametrised thickness law and a parametrised camber law. A thickness law of reference is built with the BEZIER-Parsec 3333 parametrisation described in (Salunke et al., 2014), in which geometrical parameters can be easily set and tuned. In order to stay close to the simplest thickness laws, no inflexion points are permitted. From then, the parametrised thickness law is obtained by tuning the maximum thickness value. A circular trailing edge (TE) is added so that the dimensioned aerofoil has a constant trailing edge thickness, fixed to the smallest manufacturable value shown in Table 2. Examples of thickness laws are shown in Figure 5. The camber law is obtained from a spline of order 2 constrained by three parameters: the position of the maximum of camber and the values of its tangents at the edges. Several examples are shown in Figure 6. Providing a chord value and a two-dimensional position is then sufficient to define an aerofoil with 7 parameters. Given a linear evolution, a hub aerofoil, a tip aerofoil and a height value define an entire guide fin with 15 parameters.

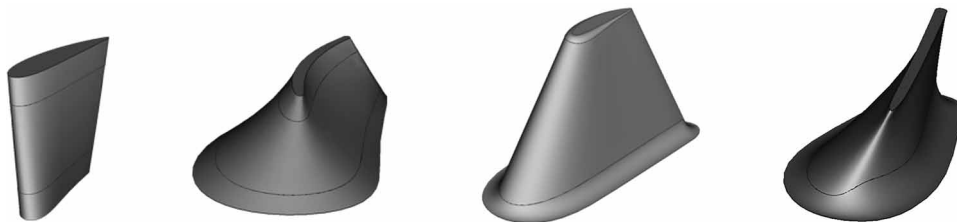


Figure 4. Examples of guide fins of various shape complexity.

Table 2. Manufacturing constraints.

Manufacturing constraint	Value
Absolute minimum fillet radius	5 mm
Absolute value of TE thickness	0.5 mm
Maximum sweep or lean angle at LE or TE	45°
Absolute minimum value of guide fins chord	25 mm
Absolute minimum guide fin height	1 mm

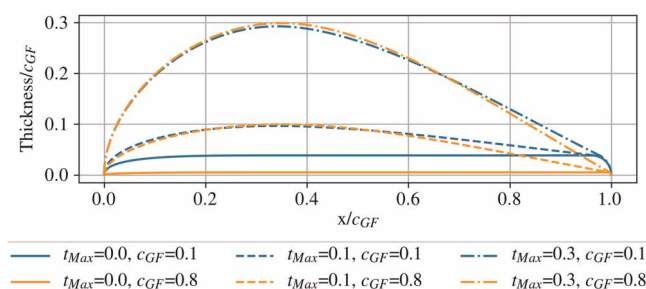


Figure 5. Thickness laws for different guide fin chords (c_{GF}) and maximum thicknesses (t_{Max}).

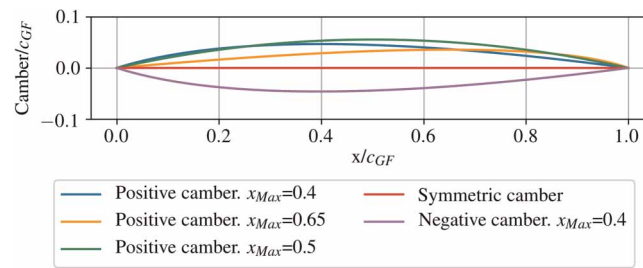


Figure 6. Camber laws for different maximum positions (x_{Max}) and tangents at the edges.

Fillets parametrisation

In the present work, fillets can have much larger radii than in conventional uses. Therefore, they can be used to either round the junctions or to deform the guide fin surface near them. The hub fillet is chosen to have a constant radius along the side surface and is therefore defined with one parameter. However, the radius of the tip fillet varies along the chord in order to avoid self-intersection. It varies from a fixed lowest value set by manufacturing constraints at the trailing edge up to a maximum value at the leading edge. A spline of order 3 is used to avoid curvature discontinuities at the LE. The maximum value is computed as the minimum radius of curvature of the tip aerofoil in its first 25% of chord. This criterion was found to correspond successfully to the largest fillet radius reachable before self-intersection in the leading edge region. The final geometry of the tip fillet can then be obtained with a single parameter, the percentage of the maximum fillet radius authorised at the tip leading edge.

Efficient design space exploration accounting for manufacturing constraints and design experience

The 17 degrees of freedom of the parametrised guide fins may lead to guide fins which are irrelevant in terms of aerodynamic expertise or do not respect manufacturing and positioning constraints (see Table 2). In order to reduce the design space to geometries of interest for the user, two new parametrisations are proposed with the following characteristics: (a) for all values of the new parameters, the associated value of the original 17 ones can be easily retrieved and (b) all geometries generated by the new parameters satisfy the manufacturing and positioning constraints. The first parametrisation involves only 4 new parameters presupposed to have a significant impact on the losses. This defines a relatively small subdomain easier to explore and mostly based on design experience. These 4 parameters correspond to the guide fin height, the inlet and outlet metal angles, and the curvilinear position on a midpitch line (see Figure 7) around a rather simple, two-dimensional aerofoil of reference. Their values is described in Table 3. The second parametrisation consists of 16 new parameters, allowing for more complex shapes. Guide fins can have very 3D geometries. Thin tip aerofoils and thin to thick hub aerofoils are considered. As tip fillet radii would be very small, no tip fillets are considered. Hub fillet radius varies between 0 and 75% of the guide fin height. Lean and sweep parameters varying between $\pm 25^\circ$ are introduced. The position of maximum camber varies in $[30\%c_{GF}, 60\%c_{GF}]$. Moreover, guide fins are forced to be relatively aligned with the local stator camber line. The angle between the tangent to the stator camber line and the x-axis is computed. The guide fin metal angles vary in $[-5^\circ, +5^\circ]$ with respect to this angle at the corresponding axial

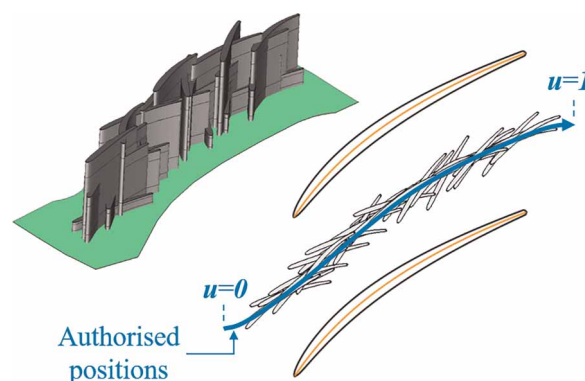


Figure 7. All guide fins of DOE-4.

Table 3. DOE-4 parameters range and value %c and % C_{GF} refer to percentages of stator and guide fin chord.

Parameter		Value
Height	∈	[0.8%c, 20%c]
LE metal angle β_1	∈	[20°, 65°]
TE metal angle β_2	∈	[0°, β_1]
Position on midpitch line u	∈	[0.14, 0.88]
Chord	=	30%c
Position of maximum camber	=	55% C_{GF}
Maximum thickness	=	4.5% C_{GF}
Radius of tip and hub fillets	=	0

positions, except for the inlet hub angle that varies in $[-20^\circ, +5^\circ]$. Finally, relatively short guide fins with a height in $[0.8\%c, 8\%c]$ are considered, with a minimum chord of $0.2c$, and the authorised positions are extended to the blue surface shown in [Figure 8](#).

Unfortunately, even these new parametrisations cannot guarantee that any geometry generated at random in these reduced design spaces will be associated with a RANS prediction. Indeed, the surface generation, the meshing process or the computation itself could fail in case of too complex geometries. In order to generate a design of experiments (DOE) which best explores the design space of admissible guide fins (i.e. with an available RANS result), an original and specific strategy for handling such computational failures is used. First, for each parametrisation, a large database of guide fins is generated using a Monte Carlo methodology and only the guide fins with viable CAD surfaces are kept. The main assumption in the algorithm used is that such large databases are representative of the set of all admissible geometries. The DOE is then built by picking a small subset which spans as best as possible the entire database. To achieve this, the “kernel herding” algorithm proposed by ([Chen et al., 2010](#)) is used. It consists in minimising the distance between the empirical distribution defined on the DOE and the one on the entire dataset. For the first parametrisation with 4 parameters, the corresponding DOE (DOE-4) with 40 geometries is shown in [Figure 7](#). For the second parametrisation with 16 parameters, the corresponding DOE (DOE-16) contains 160 geometries. 5 of them are shown in [Figure 8](#). Later in the paper, RANS results associated with each DOE are presented. Respectively 100% of the DOE-4 and 80% of the DOE-16 is successfully associated with a RANS result. These high viability rates ensure that both subdomains are indeed well explored.

Hybrid meshing strategy

In order to save computational time and to uncouple the spatial discretisation of the two geometries, the stator part is meshed separately from the guide fin part and is fixed. Attention is paid to generate these meshes consistently with one another. A structured O-4H mesh of a single channel of the baseline cascade is obtained using AutoGridV5 (Numeca). It contains approximately 1.1×10^6 hexahedral cells, and is characterised by a maximum y^+ value of 4 in the leading edge region. A symmetry plane is used at midspan. Blocks are then rearranged to centre the mesh on the channel, and to define one block of controlled dimensions, in red in [Figure 9](#). The structured O-grid block is not modified to ensure a systematic, high quality discretisation of the profile boundary layer. The red block is then replaced by an unstructured mesh containing the guide fin. This results in a hybrid mesh containing both structured and unstructured blocks. The unstructured red block is generated automatically using the software ANSA (Beta). It is made of 24 prisms layers that grow from and in a direction normal to the solid surfaces, of tetrahedra and of pyramids. Efforts are made to have elements as square as possible at the interface to enhance the quality of the pyramids. Prisms and pyramids automatically connect to the red boundaries, thus ensuring grid point coincidence. The growth rate at the interface is set to 1.2 for both volumes to ensure its continuity, yielding an unstructured block of typically 3.5×10^5 cells with a guide fin, and

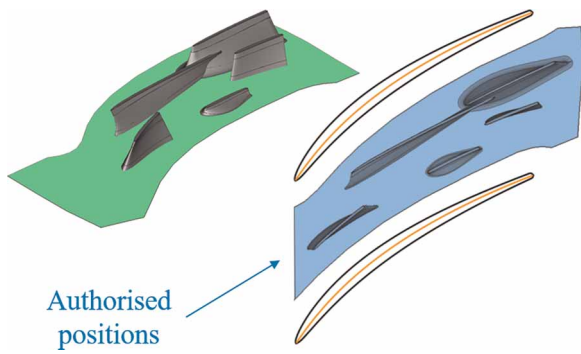


Figure 8. Several guide fins of DOE-16.

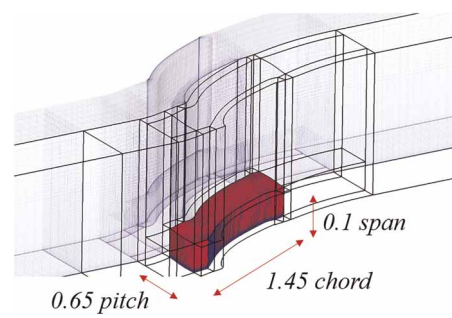


Figure 9. Unstructured block boundaries In red. Black lines: block borders. A second faded channel is added for visualisation purposes only.

c_{GF} cells without. Figure 10 shows portions of a hybrid mesh with a guide fin and illustrate the consistence of the two meshes.

CFD set up

RANS results are computed using the CFD solver elsA (ONERA). In order to validate the meshing methodology, results obtained on the fully structured mesh of reference and on the hybrid mesh without guide fin are compared in Figure 11, using the turbulence models of Spalart-Allmaras, $k-l$ of Smith and $k-\omega$ Menter BSL. The spatial scheme of Roe of order 2 is used with no limiter for variable reconstruction at interfaces. Among these three turbulence models, $k-\omega$ Menter BSL is found to best retrieve the experimental wake profiles at midspan and the downstream endwall boundary layer thickness, with both meshes. Using the hybrid mesh lowers the critical incidence by 0.2° to $i_{crit} = 4.4^\circ$. Above $i = 4.6^\circ$, the endwall losses differ by about 0.2%, but the gradient with respect to the incidence is identical. Given the sensitivity to the numerical environment, these differences are not surprising and remain acceptable. The capability of the solver elsA to perform RANS computations on hybrid meshes is therefore validated. DOE-4 and DOE-16 will therefore be evaluated using hybrid meshes, with $k-\omega$ Menter BSL.

Results and discussion

Results of the design of experiments

Respectively 40 and 129 viable guide fins are selected for the DOE-4 and the DOE-16. The present work focuses on guide fins that act on a large range of incidences, while not deteriorating too much the losses at the design incidence. As guide fins are designed to act on the near-endwall losses, it is not relevant to evaluate them at incidences where separation at midspan occurs. As a consequence, endwall losses are monitored at an incidence

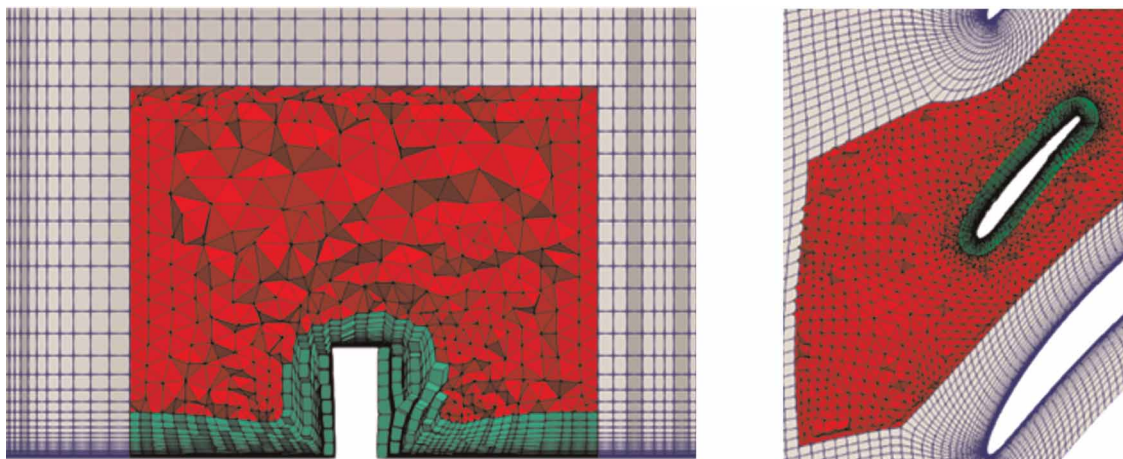


Figure 10. Portions of hybrid mesh with a guide fin White elements: hexahedra (structured part). Green elements: prisms. Red elements: tetrahedra and pyramids.

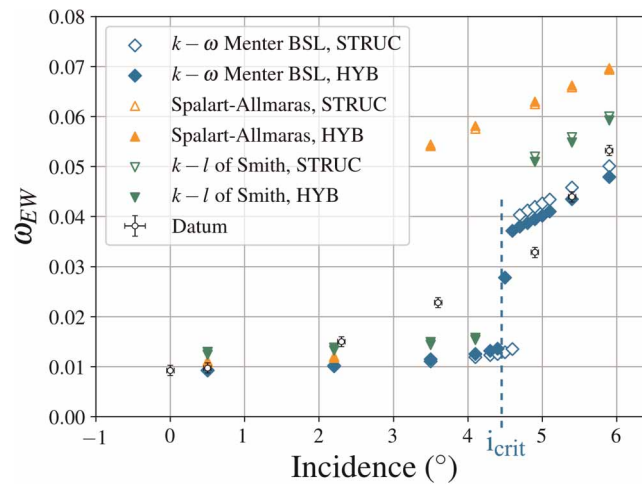


Figure 11. Evolution of the endwall losses on the measurement plane. STRUC and HYB respectively refer to results obtained using the structured ω mesh of reference and the final hybrid mesh without guide fins. The same post-processing is used for both experimental and numerical data.

near-design, $i = 0.5^\circ$, and before the midspan separation, at $i = 4.9^\circ$. Results are gathered in Figures 12 and 13, together with the RANS prediction of the baseline case for comparison purposes.

Results of DOE-4 show a widely spread cloud of points with guide fins that either deteriorate or improve the flow. No guide fin improves the flow on both objective functions compared to the baseline configuration, but several configurations dominate the others, in the Pareto sense. GF-4, in green, is particularly of interest as it significantly decreases the losses at high incidence without deteriorating too much the flow near design. Most of guide fins of the DOE-16 have a relatively low impact on the losses at near-design. This is consistent with its related design space, in which guide fins are forced to be relatively aligned with the local stator camber line. However, they are spread across a large range of losses at $i = 4.9^\circ$. For the same reasons as GF-4, GF-16 appears to be particularly interesting.

In order to assess the ability of this RANS-based set up to find efficient guide fins with two different parametrisations, GF-4 and GF-16 are selected for experimental investigations.

Experimental validation

Table 4 gathers the experimental and RANS evaluations of GF-4 and GF-16. Experimental results confirm that both reduce or have a negligible effect on the endwall losses at 0.5° , and strongly reduce these losses at 4.9° . Notably, a maximum relative loss reduction of 36% is measured with GF-4. DOE-4 and DOE-16 thus enabled to find interesting guide fins that lower the losses. However, these guide fins appear less performant at 4.9° than expected.

GF-16 is evaluated on more incidences for a more in-depth characterisation. Results are gathered in Figure 14. It appears that endwall losses are predicted to increase smoothly with the incidence. RANS predictions thus do not exhibit a critical incidence anymore, yielding an understandable over prediction of the gain in losses.

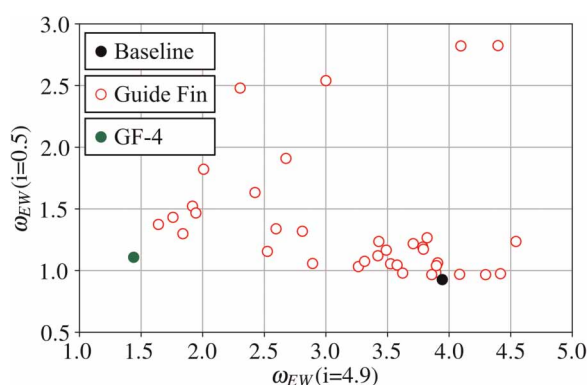


Figure 12. CFD results of DOE-4.

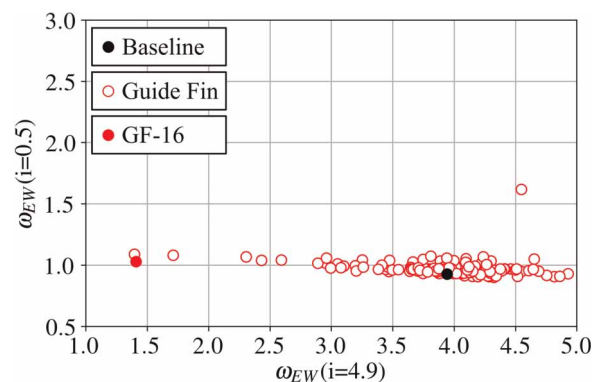


Figure 13. CFD results of DOE-16.

Table 4. Variation in endwall losses when adding GF-4 and GF-16. Predictions vs Experiments.

Incidence	Type	$\Delta\omega_{EW,GF-16}$	$\frac{\Delta\omega_{EW,GF-16}}{\omega_{EW,baseline}}$	$\Delta\omega_{EW,GF-4}$	$\frac{\Delta\omega_{EW,GF-4}}{\omega_{EW,baseline}}$
0.5	RANS	+0.10%	+12%	+0.19%	+21%
	Experiment	$-0.05\% \pm 0.1\%$	$-5\% \pm 1\%$	$+0.01\% \pm 0.1\%$	$+1\% \pm 1\%$
4.9	RANS	-3.08%	-71%	-3.01%	-70%
	Experiment	$-0.98\% \pm 0.1\%$	$-30\% \pm 1\%$	$-1.17\% \pm 0.1\%$	$-36\% \pm 1\%$

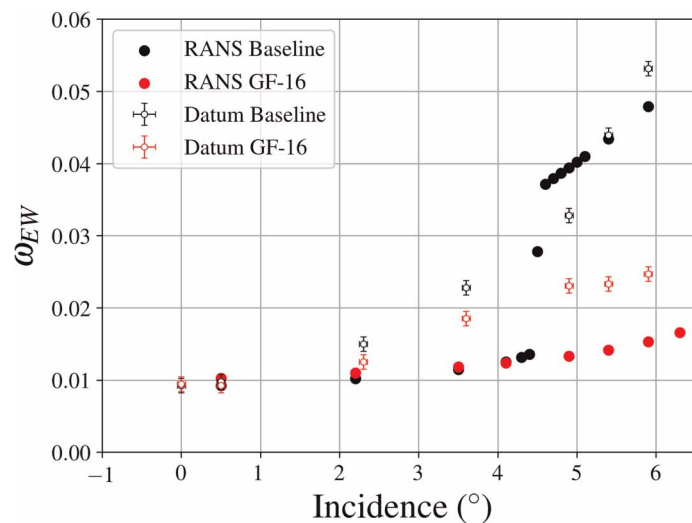


Figure 14. Evolution of the endwall losses on the measurement plane. Baseline Vs GF-16.

Moreover, experimental endwall losses are decreased not only at 0.5° and 4.9° , but on a broad range of incidence from 0° to 5.9° . Notably, a net gain of 2.06%, corresponding to a relative gain of 47% is found experimentally at 5.4° , the last incidence before the midspan profile starts separating. GF-16 thus improves the robustness to stall while not degrading near-design losses.

Figure 15 compares the loss distributions predicted by RANS and measured downstream of the cascade, with and without guide fin at 0.5° and 4.9° . In the baseline case, RANS is found to under predict the corner separation at 0.5° and to over predict it at 4.9° with respect to experimental results. However, its spatial extension seems well captured. This is typical of a flow evolution before and after the critical incidence. On the other hand, predictions with GF-16 do not exhibit such an over prediction at 4.9° . This is consistent with the smooth evolution of the endwall losses and the absence of critical incidence in that case. Moreover, specific loss patterns are retrieved, such as the low loss region framed in black at 4.9° and the signature of the guide fin tip vortex pointed out by the black arrow at 0.5° . This confirms that the refinement levels in the experimental probe mesh and the numerical hybrid mesh are consistent with one another.

The implemented numerical methodology enabled to find interesting guide fins, using RANS predictions on two incidences. Adding a guide fin that reduces the losses is found to improve the prediction of the loss distribution downstream of the cascade. Therefore, the use of RANS is proven legitimate for finding efficient guide fins. Beyond the scope of this work, RANS seems promising for an optimisation process, in which the influence of more efficient guide fins could be better predicted.

Conclusions

In this paper, a numerical methodology based on RANS predictions of parametrised guide fins was presented. It was shown that this parametrisation could be efficiently tuned to restrain the explored design space according to the user experience. This could be done either by selecting several parameters pre-supposed to have a significant

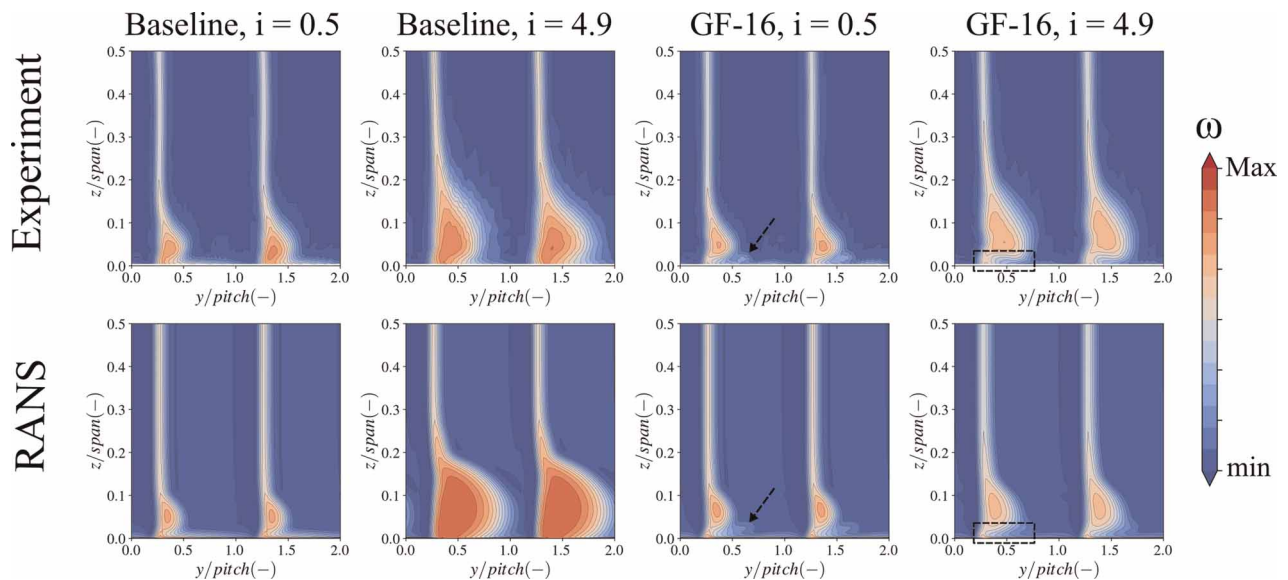


Figure 15. Total pressure losses on the measurement plane 0.2c downstream of the cascade. Black rectangle: low loss region. Black arrow: signature of guide fin tip vortex. The investigated blade is on the left.

impact on the flow, or by constraining the aerodynamic characteristics of the explored guide fins. An automated hybrid meshing process enabled to mesh guide fins of various shapes consistently with a reference structured mesh obtained with AutoGridV5. This methodology was used together with dedicated algorithms to efficiently explore the design space. In total, 169 guide fins of various geometries were evaluated with RANS. The predictions of the two best guide fins are corroborated experimentally, both on endwall losses and loss distributions downstream of the cascade. Let us underline that DOE-4 was generated by varying four parameters pre-supposed to have a major impact on the endwall losses. As GF-4 enables to lower the losses, the height, the axial midpitch position and the inlet and outlet metal angles are likely to indeed play a major role in the corner separation control.

The well-known defect of RANS, yielding the notion of critical incidence was assessed on the baseline configuration. It appeared that this defect disappears for guide fins that efficiently improve the flow, thus justifying the use of RANS predictions to design such control devices. A nonphysical over prediction of the gain in losses at high incidence directly deriving from this defect was highlighted. However, important gains at high incidence were still found experimentally without degrading the losses near design. The operability of the stator is then successfully widened by these guide fins. Notably, a relative endwall loss reduction of 47% is measured at $i = 5.4^\circ$ with GF-16.

Perspective

Further investigations will be carried out in order to understand the effects of the guide fin shape on the flow. This could involve the coupling of this methodology with an optimisation process. If predictive enough, using metamodels could help ranking the influence of each shape parameter on the endwall losses.

Nomenclature

x	Axial coordinate
y	Pitch-wise coordinate
z	Spanwise coordinate
Re	Reynolds number, based on true chord
U_∞	Upstream velocity
θ	Boundary layer momentum thickness
p_{t_∞}	Upstream total pressure
p_{s_∞}	Upstream static pressure
p_t	Downstream total pressure
c	Stator chord

c_{GF}	Guide fin chord
%c, % c_{GF}	Percentage of stator or guide fin chord
i	Incidence
i_{crit}	Critical incidence
ω_T	Integrated total pressure losses
ω_{MID}	Profile total pressure losses
ω_{EW}	Endwall total pressure losses
$\Delta\omega_{EW,GF-16}$	Endwall losses variation with respect to the baseline case when adding GF-16
DOE	Design Of Experiments
RANS	Reynolds Averaged Navier Stokes
FDM	Fused Deposition Modelling
ABS	Acrylonitrile Butadiene Styrene
LE	Leading Edge
TE	Trailing Edge
LMFA	Laboratoire de Mécanique des Fluides et d'Acoustique
ONERA	Office National d'Etudes et Recherches Aéronautiques
elsA	ensemble logiciel de simulation en Aérodynamique

Acknowledgments

The authors would like to thank Sebastien Da Veiga, Emma Croner and Etienne Tang from Safran Tech for their time and support. At Safran Engineering Services, the authors thank Philippe Biagi for his advices on the use of ANSA. At LMFA, the authors would also like to thank Sebastien Goguy, Pierre Laucher, Benoit Paoletti, Gilbert Halter and Lionel Pierrard for their advices on the experimental set up. Finally, special thanks to Ivo Dawkins, for his many discussions and for sharing his experience on the baseline configuration.

Funding sources

Safran Tech (France). CIRT (Consortium Industrie-Recherche en Turbomachine, France).

Competing interests

Gabriel Mondin declares that he has no conflict of interest. William Riéra declares that he has no conflict of interest. Pierre Duquesne declares that he has no conflict of interest. Xavier Ottavy declares that he has no conflict of interest.

References

- Chen Y., Welling M., and Smola A. (2010). Super-samples from kernel herding. In UAI10, Catalina Island, CA: AUAI Press, pp. 109–116.
- Dawkins I., Taylor J., Ottavy X., and Miller R. (2021). THE UNSTEADY TOPOLOGY OF CORNER SEPARATIONS, *Proceedings of ASME Turbo Expo 2021*, p. 17.
- Délery J. M. (2001). Robert Legendre and Henri Werlé: toward the elucidation of three-dimensional separation. *Annual Review of Fluid Mechanics*. 33 (1): 129–154. <https://doi.org/10.1146/annurev.fluid.33.1.129>
- Feng G., Ma W., Sun J., Boudet J., Ottavy X., Liu Y., Lu L., and Shao L. (2015). Large-eddy simulation of 3-D corner separation in a linear compressor cascade. *Physics of Fluids*. 27 (8): 085105. <https://doi.org/10.1063/1.4928246>
- Gessner F. B. (1973). The origin of secondary flow in turbulent flow along a corner. *Journal of Fluid Mechanics*. 58 (1): 1–25. <https://doi.org/10.1017/S0022112073002090>
- Goodhand M. N. and Miller R. J. (2012). The impact of real geometries on three-dimensional separations in compressors. *Journal of Turbomachinery*. 134 (2): 021007. <https://doi.org/10.1115/1.4002990>
- Harvey N. W. and Offord T. P. (2008). Some effects of non-axisymmetric end wall profiling on axial flow compressor aerodynamics: Part II—multi-stage HPC CFD study. In Volume 6: Turbomachinery, Parts A, B, and C. ASME Turbo Expo 2008: Power for Land, Sea, and Air, Berlin, Germany. ASME, pp. 557–569. <https://doi.org/10.1115/GT2008-50991>
- Hergt A., Dorfner C., Steinert W., Nicke E., and Schreiber H. A. (2009). Advanced Non-Axisymmetric Endwall Contouring for Axial Compressors by Generating an Aerodynamic Separator—Part II: Experimental and Numerical Cascade Investigation. Proceedings of ASME Turbo Expo 2009, p. 11.
- Hergt A., Meyer R., Liesner K., and Nicke E. (2011). A New Approach for Compressor Endwall Contouring. In Volume 7: Turbomachinery, Parts A, B, and C. Vancouver, British Columbia, Canada: ASME, pp. 177–186. <https://doi.org/10.1115/GT2011-45858>
- Hergt A., Meyer R., and Engel K. (2013). Effects of vortex generator application on the performance of a compressor cascade. *Journal of Turbomachinery*. 135 (2). <https://doi.org/10.1115/1.4006605>

- Horlock J. H., et al. (1966). Wall stall in compressor cascades. *Journal of Basic Engineering*. 88 (3): 637. <https://doi.org/10.1115/1.3645925>
- Kang S. and Hirsch C. (1991). Three dimensional flow in a linear compressor cascade at design conditions. In Volume 1: Turbomachinery. ASME 1991 International Gas Turbine and Aeroengine Congress and Exposition, Orlando, Florida, USA. ASME, p. V001T01A047. <https://doi.org/10.1115/91-GT-114>
- Lei V.-M., Spakovszky Z. S., and Greitzer E. M. (2008). A criterion for axial compressor hub-corner stall. *Journal of Turbomachinery*. 130 (3): 031006. <https://doi.org/10.1115/1.2775492>
- Ma W., Ottavy X., Lu L., and Leboeuf F. (2013). Intermittent corner separation in a linear compressor cascade. *Experiments in Fluids*. 54 (6): 1546. <https://doi.org/10.1007/s00348-013-1546-y>
- Reutter O., et al. (2017). Advanced endwall contouring for loss reduction and outflow homogenization for an optimized compressor cascade. *International Journal of Turbomachinery, Propulsion and Power*. 2 (1): 1. <https://doi.org/10.3390/ijtp2010001>
- Salunke N. P., Ahamad J. R., and Channiwalla S. A. (2014). Airfoil parameterization techniques: a review. *American Journal of Mechanical Engineering*. 2 (4): 99–102. <https://doi.org/10.12691/ajme-2-4-1>
- Sun J., Ottavy X., Liu Y., and Lu L. (2021). Corner separation control by optimizing blade end slots in a linear compressor cascade. *Aerospace Science and Technology*. 114: 106737. <https://doi.org/10.1016/j.ast.2021.106737>
- Taylor J. V. and Miller R. J. (2017). Competing three-dimensional mechanisms in compressor flows. *Journal of Turbomachinery*. 139 (2): 021009. <https://doi.org/10.1115/1.4034685>
- Zambonini G., Ottavy X., and Kriegseis J. (2017). Corner separation dynamics in a linear compressor cascade. *Journal of Fluids Engineering*. 139 (6): 061101. <https://doi.org/10.1115/1.4035876>